KERNFORSCHUNGSZENTRUM

KARLSRUHE

Juni 1970

KFK 1216

Institut für Experimentelle Kernphysik

Investigation of the Angular Correlation in the Three-Nucleon Reaction $d + p \rightarrow p + p + n$

H. Brückmann, W. Kluge, H. Matthäy, L. Schänzler, K. Wick

GESELLSCHAFT FÜR KERNFORSCHUNG M. B. H.

KARLSRUHE

KERNFORSCHUNGSZENTRUM KARLSRUHE

Juni 1970 KFK 1216

Institut für Experimentelle Kernphysik

Investigation of the angular correlation in the three-nucleon reaction d + p → p + p + n *

H. Brückmann, W. Kluge, H. Matthäy,
L. Schänzler and K. Wick

Gesellschaft für Kernforschung m.b.H., Karlsruhe

*orally presented at the Washington Meeting on Nuclear Physics April 1970 by H. Matthäy. Bulletin of the American Physical Society Ser. II, Vol. 15, No. 4, 476 (1970)

Abstract

The reaction $d + p \rightarrow p + p + n$ was investigated by kinematically complete experiments at a deuteron bombarding energy of 52.3 MeV. The aim of a systematic study was to explore the contribution of n-p and p-p FSI at many pairs of angles. The data were analyzed using the Watson-Migdal theory. The n-p and p-p scattering lengths and the cross-sections for the production of the FSI-pairs in singlet and triplet states were extracted. The scattering lengths obtained were found to be in good agreement with the values known from free nucleon-nucleon scattering. The resulting angular distributions of the singlet and triplet cross-sections turn out to be quite different. The close relation between the angular distribution for the triplet cross-section and the angular distribution of d-p elastic scattering is discussed. In separate runs kinematics were changed in order to obtain the angular distribution of the FSI-pairs in their cm-system.

I want to present some new results of a systematic investigation of the three-nucleon reaction d + p → p + p + n. This reaction was studied by coincidence experiments at many pairs of angles using the 52 MeV deuteron beam of the Karlsruhe isochronous cyclotron.

Our main interest concentrated on a thorough study of the reaction mechanism. Particularly we aimed to establish angular distributions of the three-nucleon reaction and to test the validity of the two-step reaction model rigorously.

Fig. 1 shows schematically a basic diagram, representing the essential features of the two-step reaction model. The three-particle reaction is induced by an incoming deuteron and a proton. In the first reaction step a n-p pair with low relative energy might be produced. This pair is denoted by d^*. The second reaction step accounts for a final state interaction of the n-p pair. Such a final state interaction can be observed predominantly if the kinematics of the two-detector coincidence experiment are chosen properly.

As is evidently seen from the diagram such an experiment aims to answer two main questions. Firstly the angular distribution for the production of final state interacting n-p pairs can be measured as a function of the production angle θ_{d^*}. Secondly a measurement of the angular distribution in the subsystem of the FSI nucleons should verify the reliability of the two-step reaction model. If the two reaction steps proceed independently, one expects the d^* production probability to be independent of all variables in the subsystem.

Let us now turn to the discussion of measurements which were carried out to investigate the angular distribution of the d^* production in the first reaction step. Fig. 2 gives an example of two typical map displays obtained in our coincidence experiments.

The observed events populate the whole kinematically allowed curve in the E_3, E_4 plane. E_3 and E_4 denote the energies of the two coincident protons. In the upper map display a strong enhancement of events is observed at maximum energy E_3. Just at this point the relative energy of the other proton and the neutron is zero.

The lower map display[+] is characterized by two final state peaks. It was obtained at the unique kinematical condition, where n-p pairs with zero relative energy can be observed at two different points of the kinematical curve. For the analysis the number of coincidence events was projected onto the arc length S of the kinematical curve. The arc length S is indicated schematically in the map display.

The spectrum resulting from the lower map display is shown in fig. 3. Here at this unique kinematical situation two final state peaks arise. The data were analysed using the Watson model of FSI. Both the final state interaction in the singlet and the triplet state have been taken into account. **Therefore the** experimental data allow to evaluate the two production probabilities for the formation of n-p pairs in the singlet and the triplet state separately. The upper solid curve represents the result of the Watson fit. The fit agrees excellently with the experimental data. The different contributions arising from the singlet and the triplet states are indicated by thin curves.

Such spectra were measured at ten different pairs of angles. At all these sets of angles n-p pairs were observed **with relative** energies reaching down to zero.
The resulting angular distributions for the production of singlet and triplet pairs with zero relative energy is shown in fig. 4. The three particle cross-section is given as a function of the production angle θ_d*.

[+] **see fig. 2b**

Evidently the triplet and the singlet angular distributions exhibit remarkable different shapes. Particularly it should be stressed that the triplet state angular distribution shows a surprising similarity with the angular distribution known from the elastic p-d scattering. Indeed a quantitative relation has been established which connects the matrix elements of the two processes. The cross-section of the three-particle reaction was calculated from elastic p-d scattering. The result is shown as a solid curve. The agreement with the experimental data is excellent.

Let us now turn to the second aim of our experiments. We wanted to check the reliability of the two-step reaction model. The probabilities for the singlet and triplet d^* production should depend on the angle θ_{d^*} only. They should not depend on the internal angular coordinates of the n-p subsystem. Therefore angular correlation measurements have been carried out where the angle θ_{d^*} has been kept constant but the center of mass angle in the subsystem was varied. This means that in the laboratory system the detection angle of the third particle has to be kept constant while the detection angle θ_4 of the final state interacting proton is varied.

Such angular correlation measurements have been carried out and the formula used in the analysis is shown in fig. 5.

The three-particle reaction laboratory cross-section divided by the phase space factor is given by a sum of singlet and triplet terms. X^s and X^t denote the production probabilities for the n-p subsystem in the singlet and triplet state. F^s and F^t are the corresponding enhancement factors. The particular enhancement factor used in this analysis implies the assumption that the subsystem is formed in a pure S-state. The value of X^s and X^t were determined experimentally as a function of θ_4.

A rather small variation in θ_4 corresponds to a very large variation in subsystem angular coordinate. As is seen evidently from these experimental results the production probabilities are independent on the subsystem angular coordinate. Consequently the two-step reaction model turns out to be applicable.

The applicability of the two-step reaction model was confirmed for the n-p FSI. In separate experiments we have studied the proton-proton FSI. Reasonably the model holds in the same reaction and at identical kinematical conditions also in the situation where two protons interact in the FS. Therefore one is able to investigate an anisotropy in the p-p subsystem which might be caused by contribution of higher angular momenta in the Coulomb interaction.

Fig. 6 shows an example of a map display for the effect of p-p FSI. Here the distribution of events on the kinematical curve is shown as a function of the neutron time-of-flight and the energy of the coincident proton. Contrary to the case of n-p FSI a deep minimum is observed at zero relative energy.

This difference between n-p and p-p FSI is illustrated in fig. 7. Two spectra are shown which were measured to observe p-p and n-p FSI at identical kinematical conditions. The distribution of events in the final state region was projected onto the axis E_p. E_p denotes energy of the non final state interacting free proton. While the n-p FSI exhibits the well known peak at zero relativ energy the p-p final state interaction is characterized by this deep minimum, which is due to Coulomb force. n-p and p-p scattering lengths were obtained which are in very good agreement with the values known from free nucleon nucleon scattering.

Finally we have investigated the angular distribution in the p-p subsystem by angular correlation measurements. Some of such results are shown in fig. 8. One wants to compare the p-p interaction at different subsystem angles but at the same relative energy. Therefore the spectra are given as a function of the relative energy E_{pp} of the two protons.

The solid curves indicate least square fits using a modified Migdal enhancement factor. To compare the experimental results with an isotropic angular distribution in the p-p subsystem the upper fit is plotted also in the other spectra. The agreement between the four spectra is quite well. A detailed discussion shows that the p-p FSI pair is formed in ^1S_o state predominantly but a small anisotropy observed can be explained only by taking into consideration higher angular momenta in the Coulomb interaction.

I want to finish with the conclusion that the three-nucleon reaction can be very well explained in terms of the two-step model this holds at least at many particular kinematic situations.

Figure captions

Fig. 1 Diagram representing schematically the essential features of the two-step reaction model and indicating the way to test the model by experiment.

Fig. 2 Typical experimental map-display taken from the observation of the reaction d+p → p+p+n at E_d=52.3 MeV. The distribution of events on the kinematical locus is shown as a function of the energies E_3 and E_4 of the coincident protons detected at angles θ_3=42.0° θ_4=25.3°. The strong enhancement at maximum energy E_3 is due to n-p final state interaction (FSI). The arc-length S of the kinematically allowed curve is indicated schematically.

Fig. 2b Experimental map display taken at symmetrical proton-angles θ_3=θ_4=27.7°.

Fig. 3 The spectrum resulting from the projection of the data shown in Fig. 2b on the arc-length S. The contribution of the FSI of proton 3 and 4 with the neutron (particle 5) are shown separately for the singlet and the triplet case.

Fig. 4 The angular distribution of the three-particle production cross-section of final state interacting n-p pairs with (E_{np}=0) in singlet and triplet state.
As abscissa the c.m. production angle θ_d^* as well as the lab. angle θ_p of the "free" proton are given. The solid curve results from a theoretical calculation connecting the three-particle cross-section quantitatively to the cross-section of elastic p-d scattering. (The triangle denotes a theoretical prediction for the singlet cross-section at a backward angle).

Fig. 5 The probabilities for the production of final state interacting singlet and triplet n-p pairs obtained from an angular correlation measurement. X^s and X^t are shown as a function of the lab. detection angle Θ_4 of the final state interacting proton, whereas Θ_d^* is kept fixed. The formula used to analyse the experimental data is shown at the top. F^s and F^t denote the singlet and triplet enhancement factors. ρ_{PS} is the phase-space factor.

Fig. 6 Example of observation of proton-proton FSI in the reaction $p+d \rightarrow p+p+n$ at $\Theta_p = 25.3^\circ$ $\Theta_n = 42.0^\circ$. The distribution of events on the kinematical locus is shown as a function of the proton energy E_p and τ_n the neutron time of flight. The gap in the center of the τ_n axis is caused by use of two time of flight circuits.

Fig. 7 Comparison of n-p and p-p FSI at identical kinematical conditions. The spectra result from a projection of the experimental data on the proton energy axis E_p. The values of the singlet n-p scattering-length and the p-p scattering length determined from the spectra are given.

Fig. 8 Results of the angular correlation measurement for p-p FSI. The value of the squared three-particle matrixelement (in relative units) as given by the experiment and the corresponding Watson-Migdal fits (solid curves) are shown as a function of the energy E_{pp} of the protons in their c.m. system. For comparison the 19.5° fit is plotted also in the other spectra (dashed curve). Only the full dots were included into the fitting-procedure, because for the other points the influence of the spectator-effect cannot be neglected. The minimum relative energy E_{pp} observable at the chosen kinematical conditions is indicated by special marks.

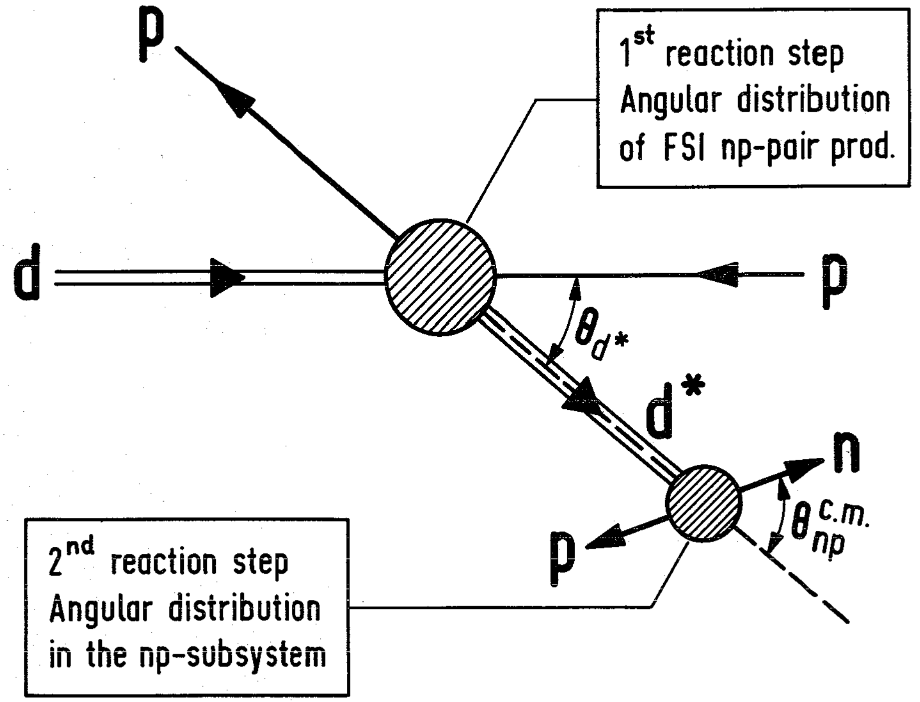
p
1st reaction step
Angular distribution
of FSI np-pair prod.
d
p
θ_{d^*}
d^*
n
$\theta_{np}^{c.m.}$
p
2nd reaction step
Angular distribution
in the np-subsystem

Fig. 1

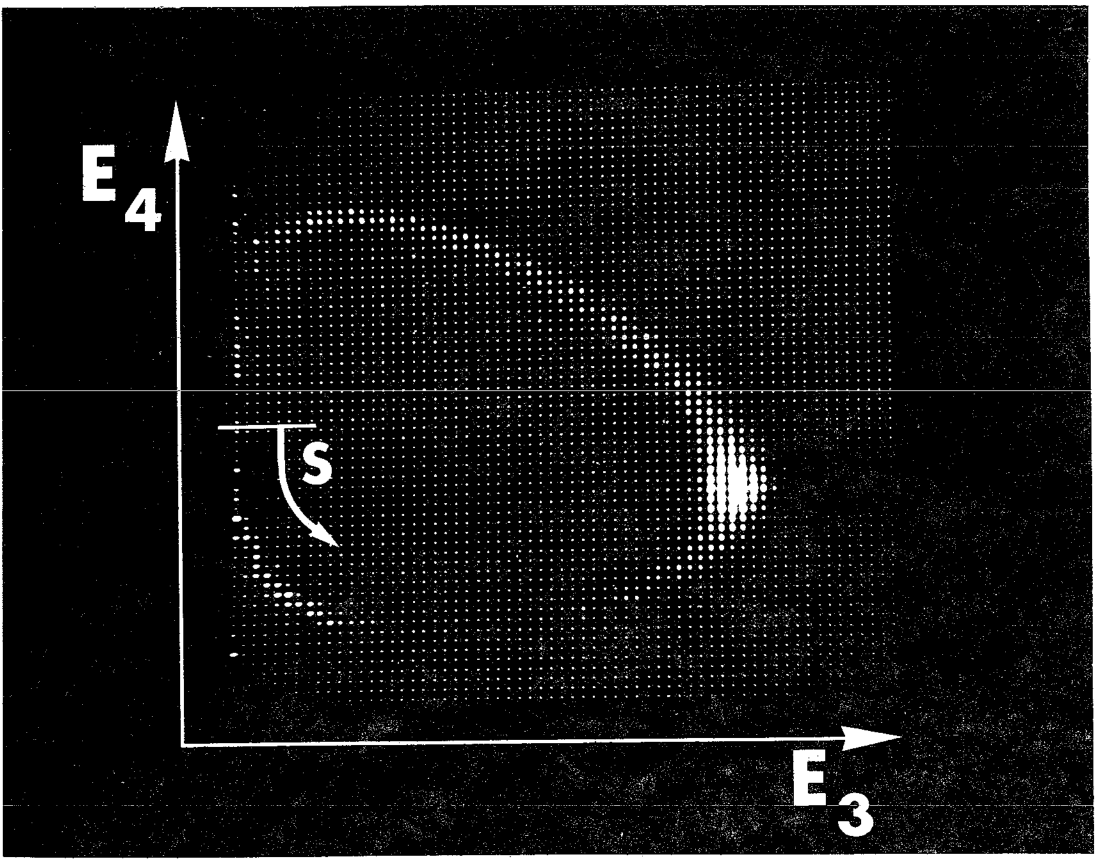
E_4
S
E_3

Fig. 2a

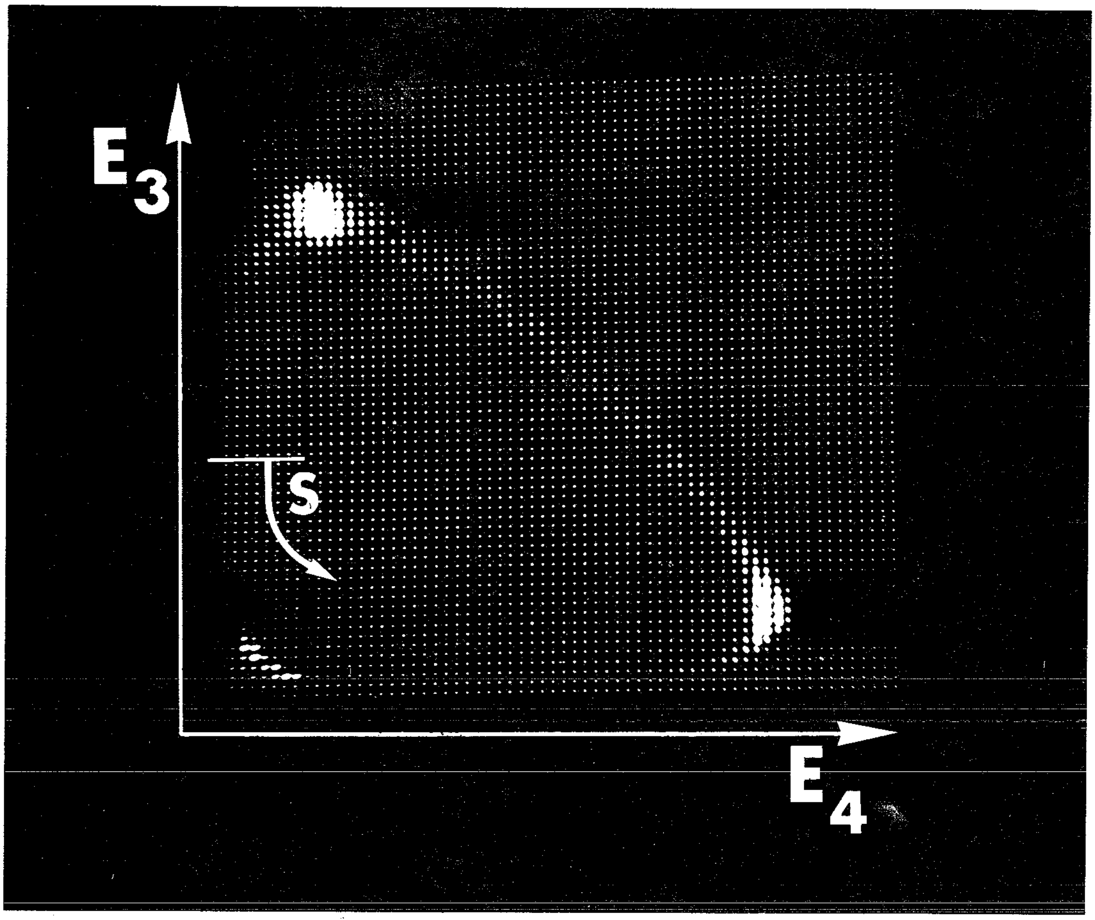
E3
S
E4

Fig. 2b

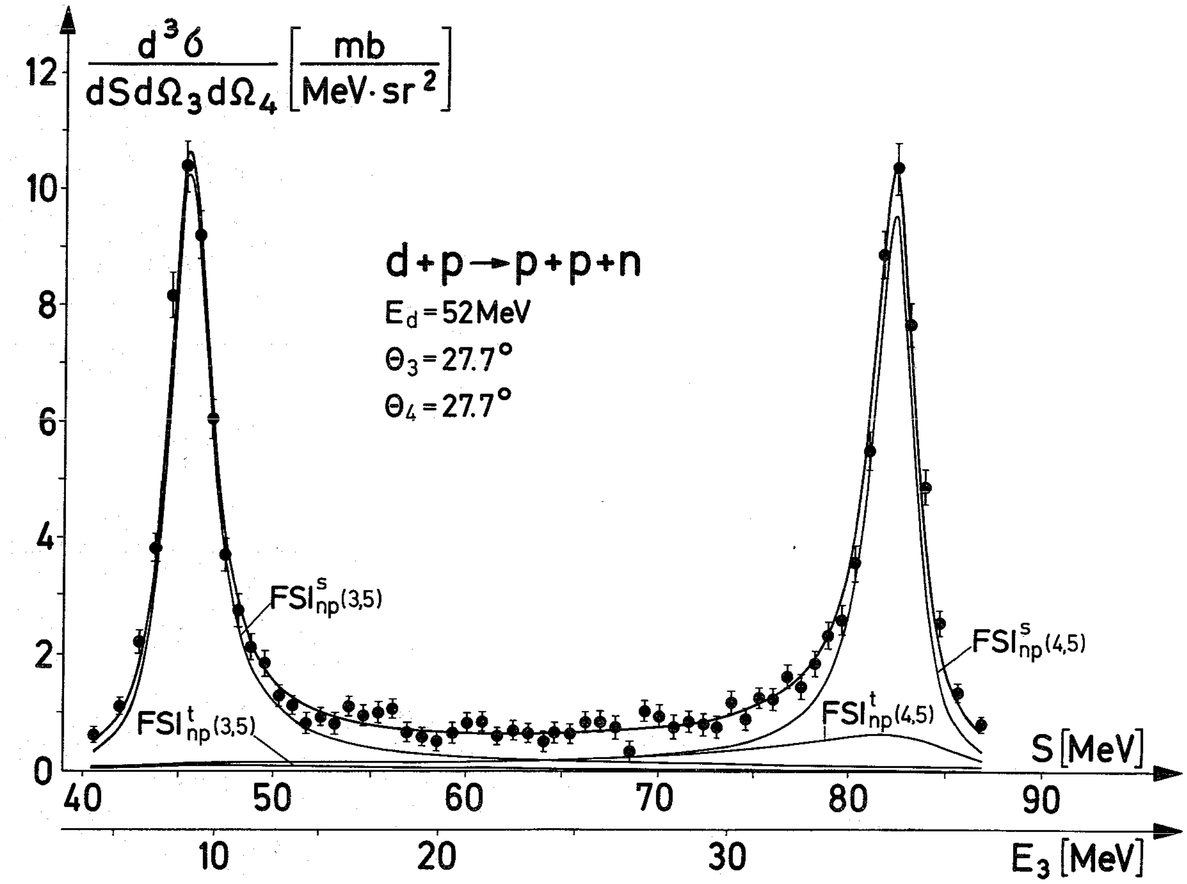
$\frac{d^3\sigma}{dS\,d\Omega_3\,d\Omega_4}\left[\frac{mb}{MeV\cdot sr^2}\right]$
12
10
8
6
4
2
0
d+p→p+p+n
E_d=52MeV
Θ_3=27.7°
Θ_4=27.7°
$FSI^s_{np(3,5)}$
$FSI^t_{np(3,5)}$
$FSI^s_{np(4,5)}$
$FSI^t_{np(4,5)}$
S [MeV]
40
50
60
70
80
90
10
20
30
E_3 [MeV]

Fig. 3

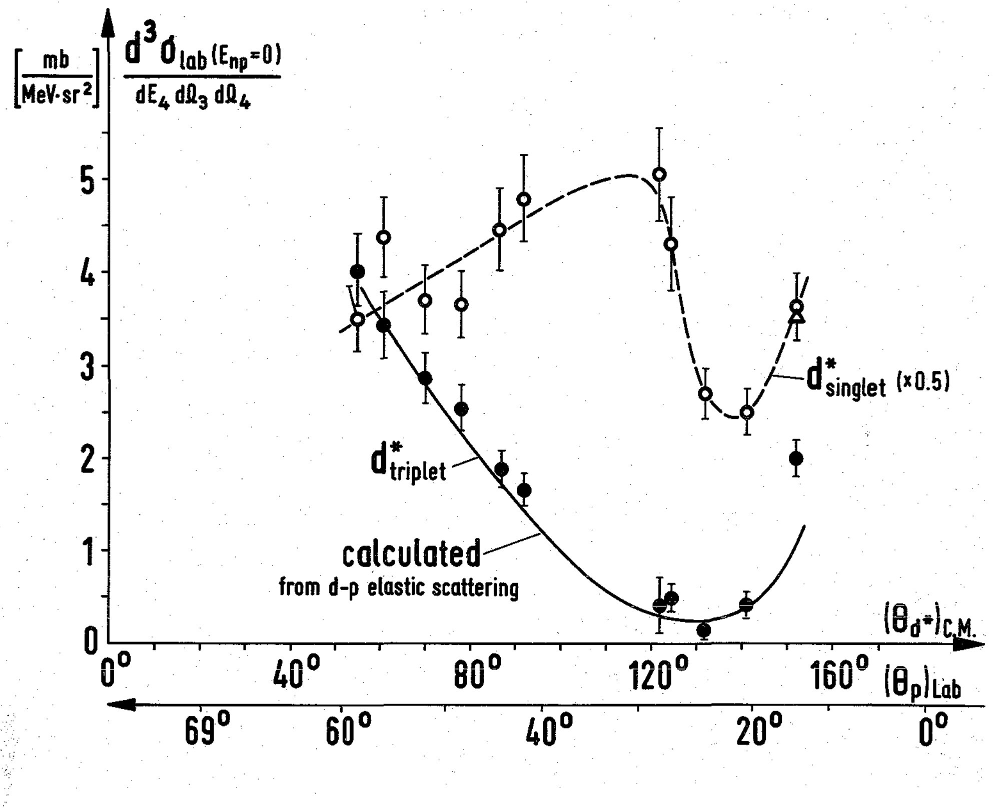
[mb / MeV·sr²]
d³σ_lab (E_np=0) / dE₄ dΩ₃ dΩ₄
5
4
3
2
1
0
d*_singlet (×0.5)
d*_triplet
calculated
from d-p elastic scattering
(θ_d*)_C.M.
0°
40°
80°
120°
160°
(θ_p)_Lab
69°
60°
40°
20°
0°

Fig. 4

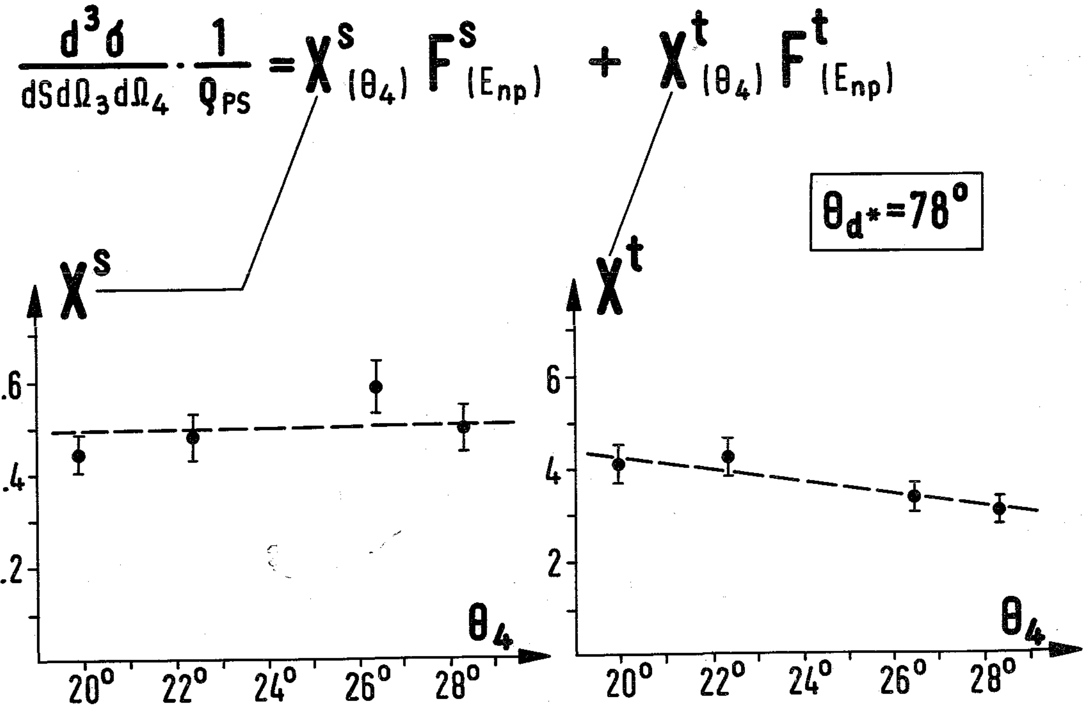
d³σ / dS dΩ₃ dΩ₄ · 1/ρ_PS = X^s_(θ₄) F^s_(E_np) + X^t_(θ₄) F^t_(E_np)
θ_d* = 78°
X^s
0.6
0.4
0.2
θ₄
20°
22°
24°
26°
28°
X^t
6
4
2
θ₄
20°
22°
24°
26°
28°

Fig. 5

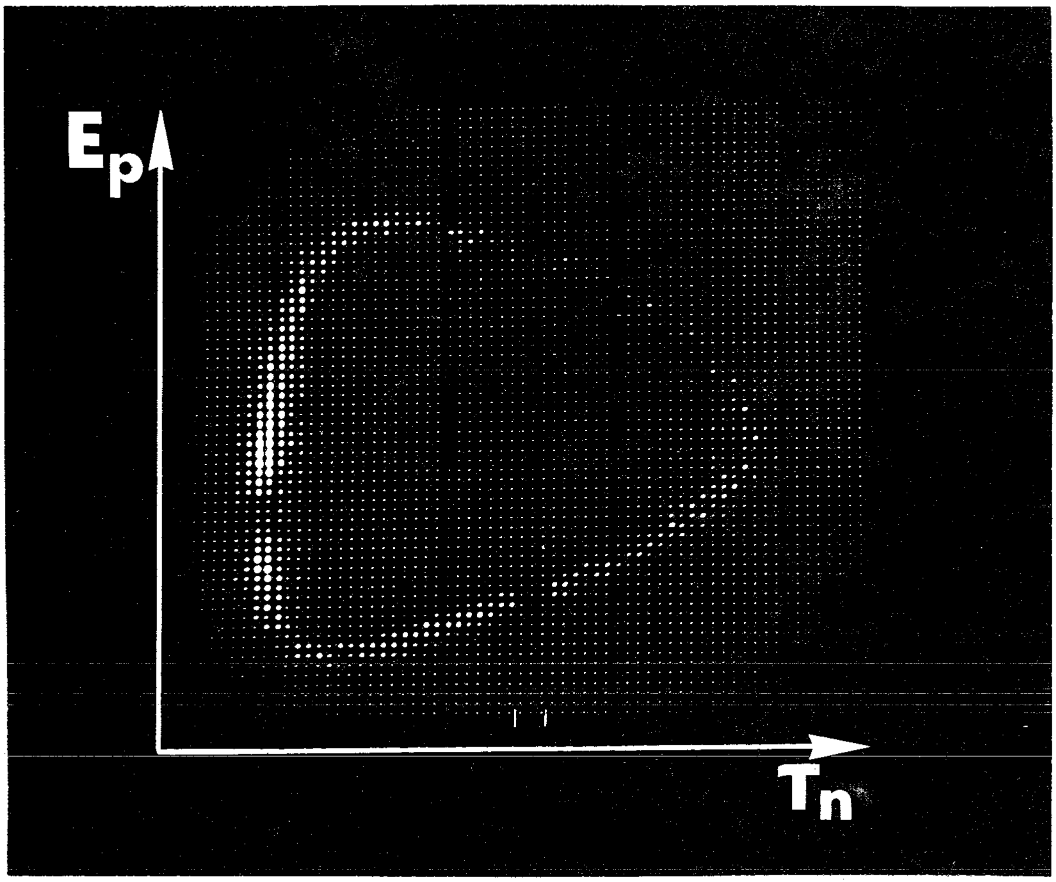
E_p
T_n

Fig. 6

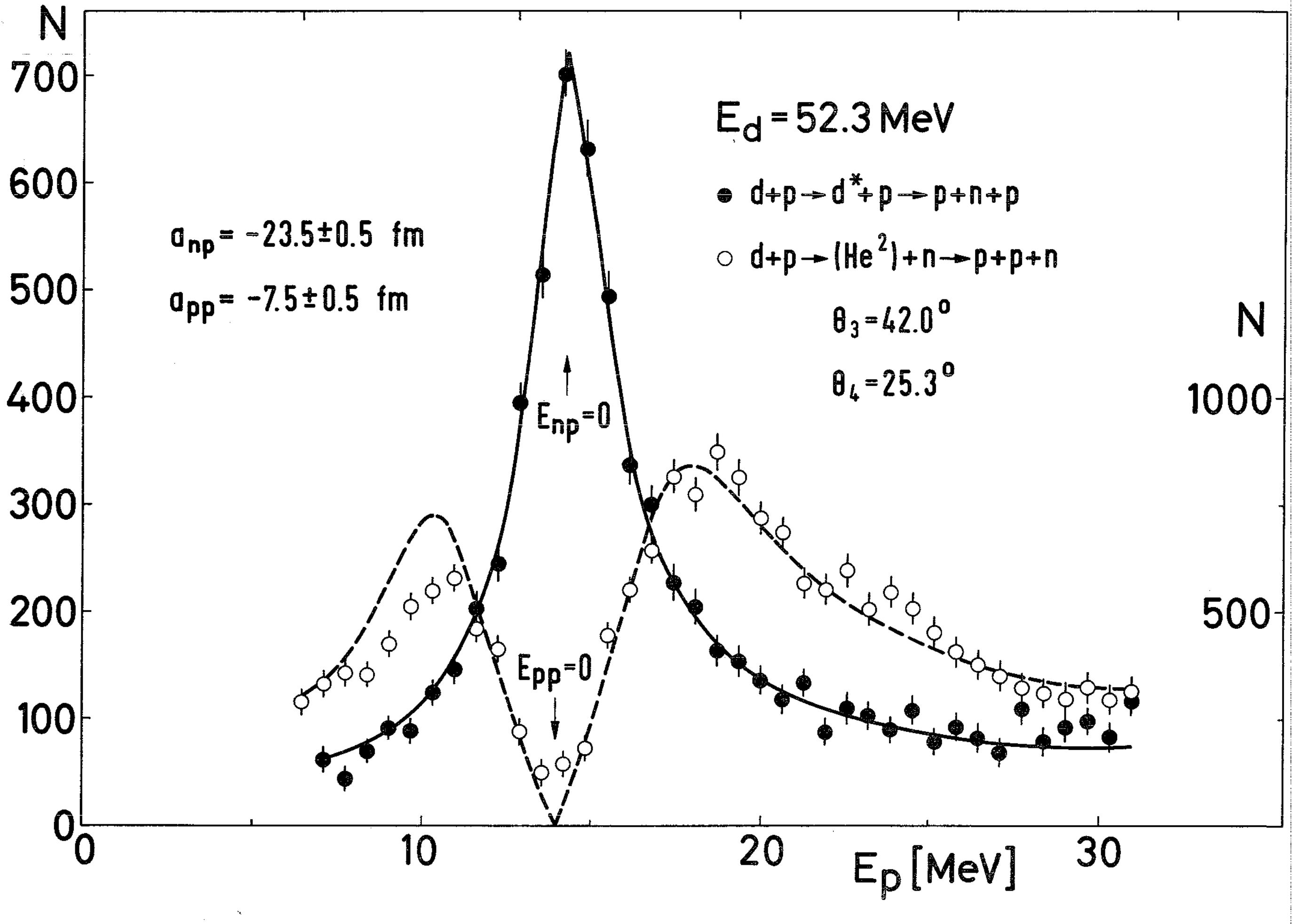
N
700
600
500
400
300
200
100
0
0
10
20
30
E_p [MeV]
N
1000
500
$E_d = 52.3$ MeV
● $d+p \rightarrow d^* + p \rightarrow p+n+p$
○ $d+p \rightarrow (He^2)+n \rightarrow p+p+n$
$\theta_3 = 42.0°$
$\theta_4 = 25.3°$
$a_{np} = -23.5 \pm 0.5$ fm
$a_{pp} = -7.5 \pm 0.5$ fm
$E_{np}=0$
$E_{pp}=0$

Fig. 7

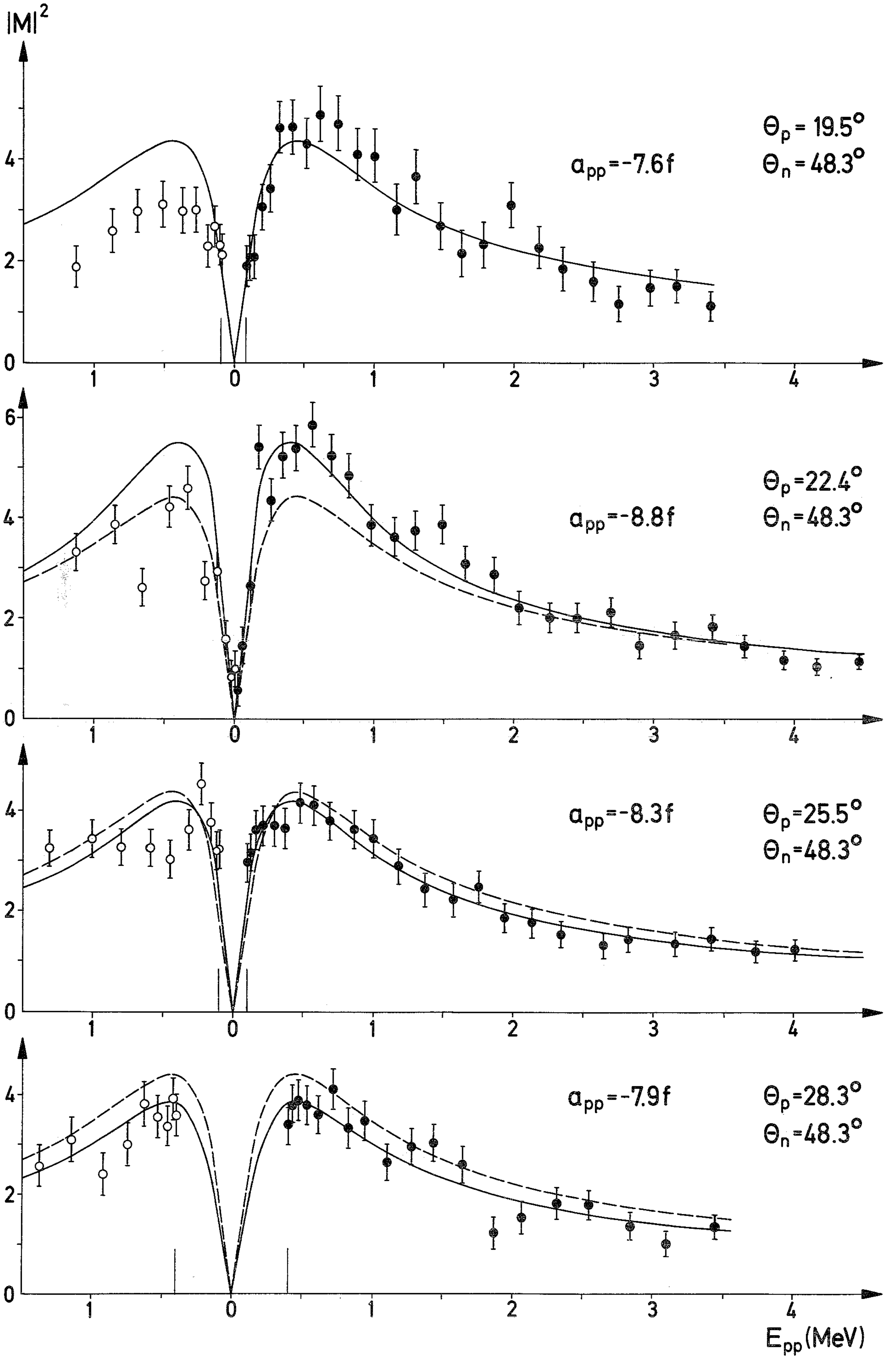
|M|^2
a_{pp}=-7.6f
Θ_p = 19.5°
Θ_n = 48.3°
a_{pp}=-8.8f
Θ_p=22.4°
Θ_n=48.3°
a_{pp}=-8.3f
Θ_p=25.5°
Θ_n=48.3°
a_{pp}=-7.9f
Θ_p=28.3°
Θ_n=48.3°
0
2
4
6
1
0
1
2
3
4
E_{pp}(MeV)

Fig. 8